phys. stat. sol. (a) **39**, 173 (1977)

Subject classification: 1.5; 13.1; 20.1; 22

Sektion Gerätetechnik der Technischen Hochschule Ilmenau[1]) *(a), VEB Elektroglas Ilmenau im KFWE (b), and Sektion Physik und Technik elektronischer Bauelemente der Technischen Hochschule Ilmenau*[1]) *(c)*

Optical Properties of Aluminium Nitride Prepared by Chemical and Plasmachemical Vapour Deposition

By

J. BAUER (a), L. BISTE (b), and D. BOLZE (c)

Aluminium nitride films are produced on fused quartz, silicon, and spinel substrates by reaction of $AlCl_3$ with NH_3 or ammonolysis of $AlCl_3 \cdot NH_3$ as well as by plasmachemical reaction of $AlCl_3$ with N_2 within a range of substrate temperatures of 700 to 1300 °C. The refraction index n, the absorption coefficient α, and the r.m.s.-surface roughness result from optical studies in the spectral range of 3.5 to 7.5 eV. The spectral dependence of optical constants yields a direct band gap $E_g = 5.9$ to 6.0 eV. Furthermore absorption bands are observed at 4.5 and 5 eV. Moreover some results for structural and electrical characterizing of films are given.

Aluminiumnitrid-Schichten werden auf Quarzglas, Silizium- und Spinell-Substraten durch Reaktion von $AlCl_3$ mit NH_3 oder Ammonolyse von $AlCl_3 \cdot NH_3$ sowie durch plasmachemische Reaktion von $AlCl_3$ mit N_2 im Substrattemperaturbereich von 700 bis 1300 °C hergestellt. Aus optischen Untersuchungen im Spektralbereich von 3,5 bis 7,5 eV ergeben sich die Brechzahl n, der Absorptionskoeffizient α und die rms-Rauhigkeit. Die spektrale Abhängigkeit der optischen Konstanten liefert einen direkten Bandabstand von $E_g = 5{,}9$ bis 6,0 eV. Außerdem werden Absorptionsbanden bei 4,5 und 5,0 eV beobachtet. Darüber hinaus werden einige Ergebnisse zur strukturellen und elektrischen Charakterisierung der Schichten angegeben.

1. Introduction

Beside such well-known insulator materials as SiO_2, Si_3N_4, and Al_2O_3 in the last few years also aluminium nitride finds an increasing interest above all because of its piezoelectric behaviour.

We have deposited AlN by means of the aluminium trichloride/ammonia process and by the plasmachemical reaction of aluminium trichloride with nitrogen.

In this paper the sample preparation and the optical properties of these AlN layers will be described.

2. Experiments for Layer Deposition

In the pyrolytic process the reactants aluminium trichloride ($AlCl_3$) and ammonia (NH_3) are supplied to the reaction zone either separately or in the form of the nearly stoichiometric complex compound $AlCl_3 \cdot NH_3$. The decrease in the standard free enthalpy change $\Delta^0 G_T^R$ for the equilibria

$$AlCl_{3(g)} + NH_{3(g)} \rightleftharpoons AlN_{(s)} + 3\,HCl_{(g)}\,, \tag{1}$$

$$AlCl_3 \cdot NH_{3(g)} \rightleftharpoons AlN_{(s)} + 3\,HCl_{(g)} \tag{2}$$

with growing temperature demonstrates their shift in favour of AlN (Fig. 1). In the experiment substrate temperatures of $T_S = 700$ to 1300 °C have been used so that

[1]) 63 Ilmenau, DDR.

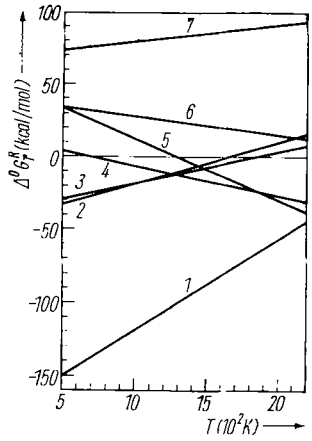

Fig. 1. Standard free enthalpie change as a function of temperature. (1) $AlCl_{(g)} + N_{(g)} \rightleftarrows AlN_{(s)} + 1/2\ Cl_{2(g)}$, (2) $AlCl_{3(g)} + N_{(g)} \rightleftarrows AlN_{(s)} + 3/2\ Cl_{2(g)}$, (3) $AlCl_{3(g)} + NH_{3(g)} \rightleftarrows AlCl_3 \cdot NH_{3(g)}$, (4) $AlCl_{3(g)} + NH_{3(g)} \rightleftarrows AlN_{(s)} + 3\ HCl_{(g)}$, (5) $AlCl_{3(g)} \cdot NH_{3(g)} \rightleftarrows AlN_{(s)} + 3\ HCl_{(g)}$, (6) $AlCl_{3(g)} + N_{(g)} \rightleftarrows AlN_{(s)} + 3Cl_{(g)}$, (7) $AlCl_{3(g)} + 1/2\ N_{2(g)} \rightleftarrows AlN_{(s)} + 3/2\ Cl_{2(g)}$

smaller outputs have to be expected for the AlN formation according to (2) compared with (1). Reaction (2) may dominate in the case of separate reactant supply to the reactor also, since there occurs an intermediary complexing (Fig. 1) at sufficient mixing of the reactants prior to the deposition process corresponding to the equilibrium position for

$$AlCl_{3(g)} + NH_{3(g)} \rightleftharpoons AlCl_3 \cdot NH_{3(g)}\,. \tag{3}$$

The thermodynamic data for $AlCl_3 \cdot NH_3$ have been determined in accordance with similar computations for the analogous gallium complex compound in [1, 2], all other values have been calculated from the thermochemical tables [3]. The reaction of aluminium trichloride with nitrogen corresponding to

$$AlCl_{3(g)} + \tfrac{1}{2}\,N_{2(g)} \rightleftharpoons AlN_{(s)} + \tfrac{3}{2}\,Cl_{2(g)} \tag{4}$$

does not lead to a deposition of aluminium nitride in neutral gas, as the standard free enthalpy change is positive also at temperatures around 1000 °C (Fig. 1). Only the utilization of the high internal energy of a plasma ("plasma-activated CVD") leads to a deposition of AlN.

Thermodynamic calculations [3] illustrate the shift of the thermodynamic equilibrium in favour of the final products as a result of

1. nitrogen dissociation,
2. recombination of the chlorine atoms,
3. aluminium trichloride dissociation (Fig. 1).

In experiments for pyrolytic preparation of AlN films vertical reactors of the type presented in Fig. 2 have been used. The substrates (111) Si, (100) Verneuil spinel $MgO \cdot 1.4\ Al_2O_3$, and fused quartz (for optical measurements) have been heated inductively with graphite susceptors coated with AlN. Convenient evaporation temperatures are $T_V(AlCl_3) = 120$ to 160 °C and $T_V(AlCl_3 \cdot NH_3) = 180$ to 400 °C, argon has been used as carrier gas. Corresponding to the $AlCl_3$ number of moles $n^0_{AlCl_3}$/h the molar ratios $n^0_{AlCl_3}/n^0_{NH_3} = 1$ to 0.001 have been realized with the help of the NH_3 flow rates. The total flow rate was varying in the limits $s_{tot} = 5$ to 220 l/h. Only at s_{tot} values above 80 l/h convective disturbances of the reactant currents homogenicity may be neglected which occur due to the high temperature gradients.

The etching behaviour of AlN-films towards H_3PO_4/H_2SO_4-mixtures in proportion 1:1 at an etching temperature of $T = 80$ °C proves that the range of the substrate temperature $T_S = 1050$ to 1250 °C supplies films of highest purity, i.e. the reactions (1) and mainly (2) proceed increasingly completely with growing temperature. The intermediary complexing at separated supply of reactants already mentioned — according to [4]

$$AlCl_3 + n \cdot NH_3 \rightleftharpoons AlCl_3 \cdot n\,NH_3\,; \qquad n = 1, 2, 3$$

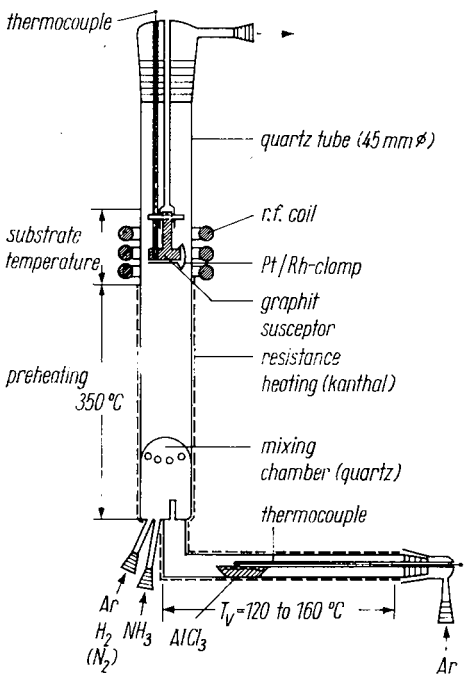

Fig. 2. Apparatus for the pyrolytic deposition of aluminium nitride

at a pre-heating temperature of $T \leqq \leqq 400$ °C — is expressed in the experimental activation energy E_A of the AlN formation process. Table 1 includes the E_A-values determined from the temperature dependence of the deposition rate for separated supply of reactants in the molar ratio 1 (a) for a reactor with the $AlCl_3$ supply pipe up to 4 cm in front of het substrate surface and (b) for the reactor shown in Fig. 2 with great mixing length as well as (c) for complex evaporation:

The activation energy for (a) is associated to the surface reaction according to (1) as rate-determining step (see also [5]) and that for (c) to the AlN formation reaction according to (2); a largely homogeneous kinetic process for the complex pyrolysis cannot be excluded even at the lower temperatures of $T_S < 1000$ °C.

The E_A-value for case (b) is decreased composed with (a) making evident that the velocity of AlN formation is compared of processes (1) and (2) as a result of the preceding reaction (3). At substrate temperatures of $T_S > 950$ to 1050 °C an increased gas phase nucleation can be seen in all cases at a corresponding decrease of the deposition rate.

The deposition rate ($R_A = 10$ to 1000 nm/min) is directly proportional to the partial pressure of the aluminium component and depends on the substrate temperature and the total flow rate within one order of magnitude under otherwise constant conditions.

The energy carrier for the plasmachemical reaction is a hf low-pressure plasma (frequency ≈ 3 MHz, pressure 0.6 Torr) produced inductively. The nitrogen plasma gas works at the same time as reacting agent and as carrier gas for the aluminium trichloride.

Table 1

experimental variant	$E_A \left(\frac{\text{kcal}}{\text{mol}}\right)$
(a) $AlCl_3 + NH_3$, $\frac{{}^0 n_{AlCl_3}}{{}^0 n_{NH_3}} = 1$	24
(b) $AlCl_3 + NH_3$, $\frac{{}^0 n_{AlCl_3}}{{}^0 n_{NH_3}} = 1$	16
(c) $AlCl_3 \cdot NH_3$	3, 5 ··· 7

$T_S = 750$ to 950 °C

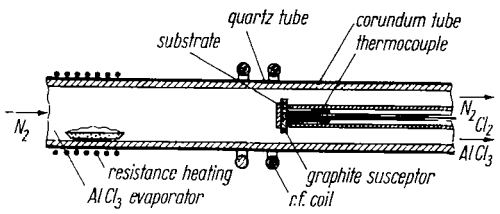

Fig. 3. Apparatus for the plasmachemical deposition of aluminium nitride

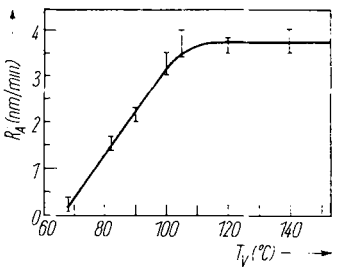

Fig. 4. Deposition rate vs. evaporator temperature. $p_{N_2} = 0.6$ Torr, $T_{Si} = 900$ °C, $t_V = 30$ min

$AlCl_3$ was heated in the evaporator up to 80 to 140 °C, this corresponds to an equilibrium vapour pressure of 0.1 to 40 Torr. The temperature of the substrate holder (AlN-coated graphite susceptor) — also heated inductively — varied in the range 800 to 1200 °C. By choosing adequate preparation parameters deposition rates of $R_A = 0.4$ to 13 nm/min have been obtained. Fig. 3 shows the reaction chamber.

The insulated films were grown on fused quartz for reflectance and transmittance studies in the energy range from 3.5 to 7.5 eV; for electrical analysis n-conducting (111)-oriented silicon with a specific resistance of $\varrho = 1$ to 10 Ω cm was used as substrate material.

The dependence of the AlN deposition rate on the evaporator temperature in the range $T_V = 80$ to 140 °C is shown in Fig. 4. Hence it follows that the deposition rate for $T_V < 100$ °C depends on the concentration of aluminium trichloride or its dissociation products, whereas at an evaporator temperature above 100 °C the reactive nitrogen particles are determining the deposition velocity.

The deposition rate in the analyzed range of film thickness $\leqq 400$ nm does not depend on the duration of the experiment. Further correlations, as i.e. the dependence of the deposition rate on the substrate temperature and the intensity of discharge are difficult to obtain because of the kind of the apparatus. The reason for that must be seen above all in the changes of substrate temperature always connected with an influence on the hf-field in the reaction zone.

3. Characterization of the Films

3.1 Structure

Hitherto pyrolytic (0001)-oriented AlN epitaxial layers could be deposited on (100) spinel $MgO \cdot 1.4\ Al_2O_3$ only in a temperature range of $T_S = 1050$ to 1250 °C [6]. There a mutual torsion of the hexagonal basal plane of 30° leads to the fact — as in the case of GaN deposition also discussed by Tempel [7] — that the reflections belonging to different azimuths occur together on the diffraction pattern.

On all other used substrate materials (e.g. Si, quartz) with both methods only (0001) fibre textures could be produced. Referring to the pyrolysis of the $AlCl_3 \cdot NH_3$ complex this is valid for temperatures from 600 to 1000 °C. But above this temperature range another preferred orientation resulted not identified uniquely so far; but also here the determined interplanar distances must be associated uniquely to AlN.

In addition to the (0001) texture still another preferred orientation could be determined at AlN films plasmachemically produced. This concerns a (11$\bar{2}$3)texture not described in literature hitherto, which occurred at evaporator temperatures below

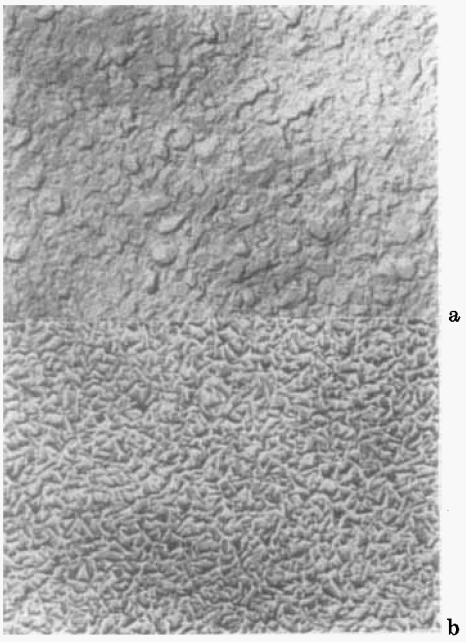

Fig. 5. Surface of AlN films on (111) silicon. a) (0001) orientation, b) (11$\bar{2}$3) orientation (11640×)

100 °C, whereas the (0001) orientation was stated at higher chloride supply. Both procedures show clearly increasing crystallite diameter on the surface with growing film thickness. Fig. 5 shows the surface (C/Pt replica) of AlN-films on (111) silicon, for which the (0001) or the (11$\bar{2}$3) surface of AlN could be determined as parallel to the substrate surface.

3.2 Electric properties

Some electric properties of the AlN-films were determined by analyzing the current–voltage and the hf-capacitance–voltage characteristics of the MIS structures (Al–AlN–Si). Through the shift of the hf-CV curve the fixed charges in the insulator were determined for flat-band conditions (N_{FB}). Whereas at samples plasmachemically produced nearly exclusively positive charges occur, there are positive and negative charges at pyrolytic AlN (see Table 2). The effective density of the charges as well as the conductivity $\varkappa$ determined from the increase of the current–voltage characteristics in the ohmic range show more favourable values for the plasmachemical process.

Table 2

	plasmachemical reaction	pyrolysis
N_{FB} (cm^{-2})	3×10^{11} to 1.3×10^{12} $U_{FB} < 0$	2 to 8×10^{12} $U_{FB} \lesssim 0$
$\varkappa$ (Ω cm)$^{-1}$ ohmic range	6.6×10^{-17} to 5.9×10^{-15} $E \leqq 1.2 \times 10^{6}$ V cm^{-1}	2×10^{-16} to 1.2×10^{-13} $E \leqq 5 \times 10^{5}$ V cm^{-1}

On the other hand first studies concerning the mechanism of current conduction in aluminium nitride yielded results greatly corresponding to each other. They led to the assumption that — as well as for silicon nitride [8] — depending on the field strength the process predominant for the charge transport is first of all hopping, at stronger fields the Poole-Frenkel mechanism or the inner field emission.

For plasmachemically produced AlN-films a nearly constant value of the relative permittivity $\varepsilon_r \approx 8.3$ occurs at an insulator diameter of about 100 nm. The increase

of the ε_r-value observed at increasing substrate temperature is attributed to an improvement of the structural perfection of the layer in good agreement with RHEED studies.

4. Optical Properties

The optical constants n and α have been determined iteratively with the help of machine computing technique from reflectance and transmittance studies at normal incidence in the energy range from 3.5 to 7.5 eV, considering multiple reflections in the substrates and the interference effect. The experimental and theoretical procedures used here have been described previously [9]. The absorption curves have been corrected by subtracting the constant background of scattered light measured in the low-energy range. This correction was very small ($\alpha \lessapprox 10^3$ cm^{-1}) for AlN produced plasmachemically. At larger scattering losses (pyrolytic AlN) the scattered light must be included, which could be attributed to the roughness of the film surfaces as has been demonstrated by electron microscopy (Fig. 5).

The roughness has a great effect on reflectance and transmittance values at smaller wavelengths (especially in the UV and VUV-region). Consequently we have to consider the roughness effect in our optical studies. For this new reflectance and transmittance equations have been derived by using the Helmholtz-Kirchhoff diffraction integral [10]. The equations consider the coherent component and have been derived supposing a normal distribution of roughness depth and by incorporating the results of Ohlidal et al. [11] for partial reflectivities.

Before determining the optical constants the intensity of surface irregularities must be known. In the region with strong absorption the interference effect and multiple reflections may be neglected and the root mean square (v. m. s.) height of the surface irregularities may be determined by the relative reflectance R/R_0 from

$$R/R_0 = \exp\left[-(4\pi\sigma/\lambda)^2\right], \tag{5}$$

where R_0 is the reflectance at normal incidence on a perfectly smooth surface, R that for a rough surface, and λ the wavelength [12].

In the range of negligibly small absorption the roughness may be calculated from the scattering losses [10]

$$S(\sigma) = 1 - T(\sigma) - R(\sigma), \tag{6}$$

where $T(\sigma)$ is the transmittance, $R(\sigma)$ the reflectance at small acceptance angles, and $S(\sigma)$ the scattered light at normal incidence on a rough surface. The last-quote method has the advantage that the reflectance of a perfectly smooth surface R_0 of the same material must not be known. The r.m.s. roughness has been determined by fitting the experimental and theoretical scattered light intensity $S(\sigma)$.

The film thickness has been determined by the continuity conditions of the closed dispersion curve [9, 10] from reflectance or transmittance studies or from the interference maximum or minimum at films with very rough surfaces.

Fig. 6 and 7 show n and α as a function of the wavelength λ and energy $\hbar\omega$, respectively, for these AlN thin films.

The dependence of r.m.s. roughness σ on the film thickness — determined by measuring the relative reflectance R/R_0 and the scattered light intensity $S(\sigma)$ — is shown in Fig. 8. There is a good agreement between the method of Porteus [12] and the measuring results of the scattered light.

We have ascertained that the absorption in the band edge region ($\hbar\omega \gtrapprox E_g$) can be expressed by the relation

$$n\alpha\hbar\omega = B(\hbar\omega - E_g)^{1/2}, \tag{7}$$

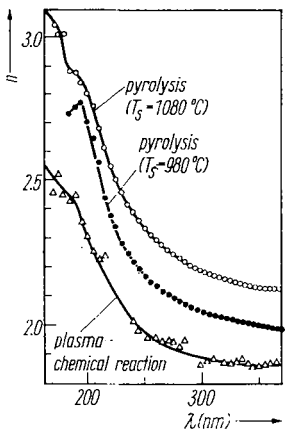

Fig. 6. Spectral dependence of the refraction index

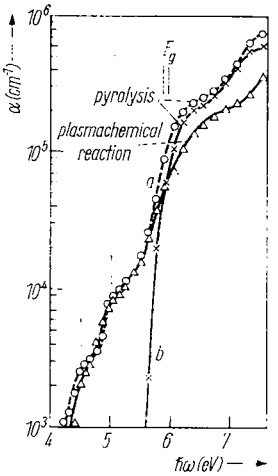

Fig. 7. Optical absorption vs. photon energy. (a) without consideration of surface roughness, (b) with consideration of surface roughness

where α is the absorption coefficient, n the refraction index, E_g the optical band gap energy, and B a constant. Relation (7) was derived by Smith [13] assuming only direct interband transitions with simple parabolic bands.

The constant B contains the oscillator strength or the optical matrix element and the reduced effective mass. Thus the experimental results refer to a direct band gap and show insignificant deviations for various preparation methods: E_g = 5.9 to 6.0 eV (see Table 3). These results show a good agreement with literature [14 to 17]. The

Table 3

method	E_g (eV)	B (10^6 cm^{-1} eV$^{1/2}$)	$\partial E_g/\partial T$ (10^{-4} eV K^{-1})
pyrolysis	5.93	5.0	− 2.8
plasmachemical reaction	6.00	3.2	− 2.5
deviation incl. reproducibility	$\lessapprox \pm$ 0.02	$\lessapprox \pm$ 0.1	$\lessapprox \pm$ 0.5

theoretical calculations of band structure associate this value of the band edge to $\Gamma_{1.6} \rightarrow \Gamma_1$ transitions in the Brillouin zone [18]. The analysis of the dependence of

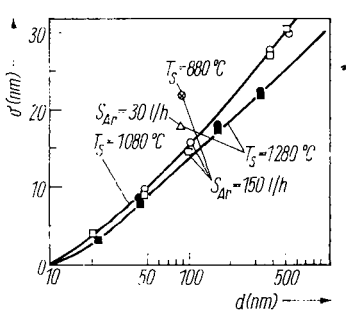

Fig. 8. Surface roughness vs. thickness. ■□ S measurements; ●○ $R = R_0 \times \exp[-(4\pi\sigma/\lambda^2)]$

absorption on the photon energy shows that there is a good agreement with the theory of a direct edge (equation (5)) in the range from about 6 to about 6.6 eV.

There is an increase of absorption at $\hbar\omega \approx 6.6$ eV, which may be explained by direct transitions between non-parabolic bands and/or by transitions in the direction T of the Brillouin zone ($\Gamma_3 - \Gamma_1 = 6.7$ eV and $K_2 - K_3 = 6.6$ eV [18]).

Furthermore the shape of the absorption curves shows that a maximum can be expected at $\hbar\omega \gtrapprox 7.5$ eV. This peak is explained by the so-called Van-Hove singularities in the joint density of states, which occur by transitions in the direction S of the Brillouin zone ($A_{1,3} - A_{5,6} = 7.5$ eV [18]). Thus the measured values show a good agreement with the theoretical values of Sobolev [18]. Moreover, the change of the band edge was measured at the temperature of liquid nitrogen. The change of the energy gap may be compared with that of other III–V compounds [19 to 21].

Besides the band edge absorption bands have been observed at 4.5 and 5.0 eV. These bands have relatively high absorption coefficients for plasmachemically produced AlN and reactively sputtered AlN [22] and are little structured. For pyrolytic aluminium nitride — considering the surface roughnesses — these bands could scarcely be noticed (see curve b, Fig. 7).

The dispersion curves show singularities according to Stern's consideration [23], which emphasize the view that AlN has a direct band gap at about 6.0 eV.

The smaller refraction indexes, the higher band absorption, and the smaller absorption coefficients at insignificant change of the band gap of the AlN plasmachemically produced may be attributed to several effects. Excess Al could be responsible for this. But probably this effect appears at reactively sputtered AlN only, since the band gap is smaller and the refraction index and the band absorption are higher [22]. It is more likely that a decrease of density dependent on the method of preparation interprets these optical properties well, especially as for Si_3N_4-films at nearly equal preparation similar properties have been observed [22, 24].

This result can be obtained with the help of the sum rules [25] or the dispersion relations [20] for determining the plasma frequency ω_p which is proportional to the density. Since E_g can be regarded as nearly constant there follows a decrease of ω_p directly from the sum rules or the dispersion relations at a decrease in refraction index, and also in density. This decrease in density, as well as the strength of the absorption bands and the values of refraction index may occur by structure defects caused by oxygen impurities [26], N–H and Al–Cl bondings [17], and nitrogen deficiencies, which may be associated directly with a built-in surplus of argon [27].

N deficiency and Ar built-in surplus may cause — as published in [27] — large internal electric fields in the vicinity of nitrogen vacancies, i.e. there is a shift of the absorption edge to lower energies (Franz-Keldysh effect). This effect will not occur at AlN produced by plasmachemical reaction, since nitrogen has been used as carrier gas. But it could explain the smaller band gaps for pyrolytic AlN and it has shown that for different preparation conditions (e.g. substrate temperature, see Fig. 6) the refraction index reacts more sensitively and thus changes in density caused by the above-mentioned effects explain largely the optical properties of AlN samples.

The inhomogeneities also contribute to the decrease of the refraction index shown by the strong discontinuities in the dispersion curves of AlN produced by plasmachemical reaction (see Fig. 6 and [22, 24]). From the contrast reduction of interference a depth of the inhomogeneity of about 100 nm for the samples produced plasmachemically may be estimated [22]. This result correlates with the results given in Section 3.

Fig. 8 shows the dependence of surface roughnesses on the film thickness, the flow rate S_{Ar}, and the substrate temperature T_S. These properties may be explained with

the growing cross-sectional area of the single crystallites with increasing film thickness (columnar growth). Furthermore, it could be noted that this sectional area decreases with growing temperature and flow rate of Ar.

References

[1] V. S. Ban, J. Electrochem. Soc. **119**, 761 (1972).
[2] H. L. Friedman and H. Taube, J. Amer. Chem. Soc. **72**, 2236 (1950).
[3] P. V. Gurvič, Termodin. svoistv indiv. vešč., Izd. Akad. Nauk SSSR, Moskva 1962.
[4] A. J. Noreika and D. W. Ing, J. appl. Phys. **39**, 5578 (1968).
[5] A. Shintani and S. Minagawa, J. Crystal Growth **22** (1974).
[6] H. Arnold, L. Biste, D. Bolze, and G. Eichhorn, Kristall und Technik **11**, 17 (1976).
[7] A. Tempel, W. Seifert, J. Hammer, and E. Butter, Kristall und Technik **10**, 747 (1975).
[8] S. M. Sze, J. appl. Phys. **38**, 2951 (1967).
[9] J. Bauer and M. Riemann, Wiss. Z. TH Ilmenau **20**, 181 (1974).
[10] J. Bauer, Exp. Techn. Phys., to be published.
[11] I. Ohlidal, K. Navrátil, and F. Lukeš, J. Opt. Soc. Amer. **61**, 1630 (1971).
[12] J. O. Porteus, J. Opt. Soc. Amer. **53**, 1394 (1963).
[13] R. A. Smith, Wave Mechanics of Crystalline Solids, Chapman and Hall, London 1961.
[14] J. Pastrnák and L. Roskovcová, phys. stat. sol. **26**, 591 (1968).
[15] G. A. Cox, D. O. Cummins, K. K. Kawabe, and R. H. Tredgold, J. Phys. Chem. Solids **28**, 543 (1967).
[16] V. I. Donetskikh, A. A. Pletyuskin, J. U. Popov, N. G. Slavina, and V. V. Sobolev, Dokl. Akad. Nauk SSSR **189**, 764 (1969).
[17] T. L. Chu and R. W. Kelm, J. Electrochem. Soc. **122**, 995 (1975).
[18] V. V. Sobolev, Fiz. tverd. Tela **12**, 2484 (1970).
[19] E. J. Johnson, Absorption near the Fundamental Edge, in: Semiconductors and Semimetals, Vol. 3, Ed. R. K. Willardson and A. C. Beer, Academic Press, New York/London 1967 (p. 125).
[20] T. S. Moss, Optical Properties of Semiconductors, Butterworth, London 1961.
[21] Y. F. Tsay, S. S. Mitra, and J. F. Vetelino, J. Phys. Chem. Solids **34**, 2167 (1973).
[22] J. Bauer, Optische Untersuchungen an dielektrischen Schichten (Si_3N_4, AlN), XX. Internat. Wiss. Kolloquium, TH Ilmenau 1975 (C2, p. 115).
[23] F. Stern, Phys. Rev. **133**, A 1653 (1954).
[24] J. Bauer, phys. stat. sol. (a), to be published.
[25] D. L. Greenway and G. Harbecke, Optical Properties and Band Structure of Semiconductors, in: The Science of the Solid State, Vol. 1, Ed. B. R. Pamplin, Pergamon Press, New York 1968.
[26] J. Pastrnák and L. Roskovcová, IX. Internat. Conf. Phys. of Semiconductors, Vol. 2, Moscow 1968 (p. 1185).
[27] A. J. Noreika and M. H. Francombe, Proc. Internat. Conf. on Thin Films **6**, 722 (1969).

(Received Augugst 20, 1976)